

1 **Chemistry contribution to stratospheric ozone depletion after the**
2 **unprecedented water rich Hunga Tonga eruption**

4 **Authors:** Jun Zhang^{1*}, Douglas Kinnison¹, Yunqian Zhu^{2,3}, Xinyue Wang¹, Simone Tilmes¹,
5 Kimberlee Dube⁴, William Randel¹

7 **Affiliations:**

8 ¹Atmospheric Chemistry Observations & Modeling Laboratory, National Center for Atmospheric
9 Research, Boulder, CO, USA

10 ²Cooperative Institute for Research in Environmental Sciences, University of Colorado Boulder,
11 Boulder, CO, USA, 80309

12 ³Chemical Sciences Laboratory, National Oceanic and Atmospheric Administration, Boulder,
13 CO, USA, 80305

14 ⁴Institute of Space and Atmospheric Studies, University of Saskatchewan, Saskatoon, SK,
15 Canada

16 *Corresponding author: Jun Zhang (jzhan166@ucar.edu)

19 **Key Points:**

- 21 ● Nudged chemistry-climate model simulations are used to quantify the chemistry impact on
22 the stratospheric ozone following the Hunga Tonga-Hunga Ha'apai eruption.
23 ● The modeled ozone and nitrogen oxides anomalies show a good agreement with satellite
24 observations.
25 ● Chemistry contributes to 6% and 20% ozone depletion at mid-latitudes and Antarctica,
26 respectively.

28 **Abstract**

30 Following the Hunga Tonga–Hunga Ha’apai (HTHH) eruption in January 2022, stratospheric
31 ozone depletion was observed in the Southern Hemisphere mid-latitudes and Antarctica during the
32 2022 austral wintertime and springtime. This eruption injected sulfur dioxide and unprecedented
33 amounts of water vapor into the stratosphere. This work examines and quantifies the chemistry
34 contribution of the volcanic materials to the ozone depletion using chemistry-climate model
35 simulations with nudged meteorology. Simulated 2022 ozone and nitrogen oxides (NO_x)
36 anomalies show a good agreement with satellite observations. We find that chemistry only
37 contributes up to 6% and 20% ozone destruction at mid-latitudes wintertime and Antarctic
38 springtime respectively. The majority of the ozone depletion is attributed to the internal variability
39 and dynamical changes forced by the eruption. Both the simulation and observations show a
40 significant NO_x reduction associated with the HTHH aerosol plume, indicating the enhanced
41 dinitrogen pentoxide hydrolysis on sulfate aerosol.

44 **Plain language summary**

45
46 The January 2022 eruption of the Hunga Tonga-Hunga Ha'apai underwater volcano injected a
47 large amount of water vapor (H_2O) and moderate amounts of sulfur dioxide (SO_2) into the
48 stratosphere. Stratospheric ozone losses were observed following the eruption in the Southern
49 Hemisphere (SH) mid-latitudes and Antarctica during the 2022 austral wintertime and springtime.
50 The ozone layer in the stratosphere protects Earth's human being and biosphere from harmful
51 ultraviolet light by absorbing the harmful portion of the radiation from the sun. We use computer
52 simulation in this study to examine the impacts of chemical processes on the ozone layer from the
53 volcanic materials. We find that chemistry is contributing up to 6% and 20% of the ozone reduction
54 at SH mid-latitudes winter and Antarctic spring respectively. The majority of ozone changes are
55 due to transport and dynamical processes from internal variability in the climate system and forced
56 response by the HTHH eruption.

57
58 **1. Introduction**
59

60 It has been long known that explosive volcanic eruptions can cause stratospheric ozone depletion
61 by injecting sulfate and its precursor SO_2 into the stratosphere, which enhances aerosol surface
62 areas for heterogeneous chemistry (Hofmann & Solomon, 1989; Portmann et al., 1996; Kinnison
63 et al., 1994; Solomon et al., 1996, 1998). Observations have shown that Antarctic ozone depletion
64 was enhanced after the major eruption of Mount Pinatubo in the early 1990s with injections of ~ 18
65 Tg sulfur dioxide (SO_2) (e.g., Read et al., 1993; Krueger et al., 1995; Solomon et al., 2005). Even
66 the moderate magnitude volcanic eruption of Calbuco in 2015, which injected 0.4 Tg of SO_2 ,
67 exacerbated ozone depletion, producing a record-breaking October ozone hole that lasted late into
68 the season (Solomon et al., 2016; Ivy et al., 2017; Stone et al., 2017; Zhu et al., 2018).

69
70 The January 2022 Hunga Tonga–Hunga Ha’apai (HTHH) eruption was an unprecedented
71 underwater volcanic event of the modern era, which injected volcanic materials to altitudes up to
72 58 km in the mesosphere (Carr et al., 2022; Proud et al., 2022). Unlike land-based volcanoes such
73 as Mount Pinatubo and Calbuco, HTHH injected about 150 Tg of water (H_2O) (Xu et al., 2022;
74 Millán et al., 2022) along with 0.4 to 0.5 Tg SO_2 into the stratosphere (Carn et al. 2022; Taha et
75 al., 2022). This H_2O injection increased the global stratospheric water burden by more than 10%
76 (Vömel et al., 2022; Khaykin et al., 2022; Randel et al., 2023). The additional source of H_2O can
77 impact the ozone chemistry by altering the HOx chemical cycles, heterogeneous reaction rate, and
78 the Polar Stratospheric Cloud formation (PSCs) (Solomon et al., 1997; Anderson et al., 2012). In
79 addition, volcanic aerosols provide extra surface area density (SAD) for heterogeneous reactions
80 affecting ozone chemistry, and suppressing the NOx-Ox cycles (defined later in Section 3.2) (Tie
81 and Brasseur, 1995).

82
83 Previous studies have utilized the chemistry-climate model Community Earth System Model
84 Version 2 (CESM2) with Whole Atmosphere Community Climate Model Version 6 (WACCM6)
85 to simulate the dispersion and evolution of aerosol and water plumes after the HTHH eruption
86 (Zhu et al., 2022; Wang et al., 2023, Lu et al., 2023). WACCM6 simulations reproduced the
87 Microwave Limb Sounder (MLS) observed evolution of the H_2O throughout 2022 and the
88 stratospheric cooling and circulation changes as seen by European Center for Medium Range
89 Forecasts ERA5 reanalysis (Wang et al., 2023). Zhu et al. (2022) found that the additional water

vapor increases hydroxide, halves the sulfur dioxide lifetime, promotes faster sulfate aerosol formation as seen by Cloud-Aerosol Lidar and Infrared Pathfinder Satellite Observation (CALIPSO) and The Ozone Mapping and Profiler Suite Limb Profiler (OMPS-LP), and leads to the increased aerosol optical depth and radiation effect. The persistent perturbations in H₂O and aerosol due to HTHH plumes in the SH stratosphere throughout 2022 draw attention to exploring the SH stratospheric ozone response.

Lu et al. (2023) explored the ozone response to the HTHH eruption considering 0.4 Tg SO₂ emission but ignored the large H₂O injection. Wang et al. (2023) simulated large stratospheric ozone anomalies in mid-latitudes and Antarctica in 2022 as observed by MLS. Manney et al. (2023) looked into the nitrous oxide anomalies with ozone and suggested that transport plays a role in the ozone reduction. However, the relative effects of chemistry and dynamics on these ozone anomalies has not been quantified. This work aims to examine and quantify the chemical ozone depletion and the associated chemical processes in the wake of HTHH. We isolate the ozone impact owing to chemistry by nudging the model dynamics to meteorology analysis fields.

2. Data and Model

2.1 Microwave Limb Sounder (MLS)

The MLS instrument was launched on NASA's EOS Aura satellite on July 15, 2004. For the past 19 years, MLS has provided a uniquely comprehensive suite of daily global measurements for studying lower stratospheric chemical processing. MLS Version 5.0 data is used in this work. The standard product for O₃ is derived from MLS radiance measurements near 240 GHz; the O₃ data and its validation are described by Livesey et al. (2020). The useful data range is from 261 hPa up to 0.001 hPa. Here the O₃ data used are compiled into a daily zonal means at a resolution of 2.5° latitude from 2004 to 2022. Anomalies for 2022 shown in this study are calculated based on climatology background from 2007 to 2021, as the model simulations started from 2007.

2.2 Optical Spectrograph and InfraRed Imager System (OSIRIS)

The Optical Spectrograph and InfraRed Imager System (OSIRIS) has been in sun-synchronous orbit on the Odin satellite since 2001 (Llewellyn et al., 2004; Murtagh et al., 2002). The optical spectrograph scans the atmospheric limb to measure vertical profiles of limb-scattered solar irradiance between 275 and 810 nm. There are between 100 and 400 profiles per day, depending on the time of year and the scanning range. Only the descending node measurements are considered here due to a drift in the orbit that has caused inconsistent ascending node sampling over the course of the mission. We use NO_x from version 7.2 of the OSIRIS retrieval, which is described and validated in Dubé et al. (2022). The OSIRIS NO₂ observations are converted to NO_x using the PRATMO photochemical box model (Prather and Jaffe, 1990; McLinden et al., 2000), following the process in Dubé et al. (2020). PRATMO is also used to scale the OSIRIS measurements to a common local solar time of 12:00 pm in order to account for variations in the measurement time caused by the processing satellite orbit, which is described in Dubé et al. (2020).

2.3 Whole Atmosphere Community Climate Model (WACCM)

The CESM2/WACCM6 was used to conduct the numerical experiments. This state-of-the-art chemistry-climate model extends from the Earth's surface to approximately 140 km and includes comprehensive troposphere-stratosphere-mesosphere-lower-thermosphere (TSMLT) chemistry (details described in Gettelman et al., 2019). WACCM6 includes a prognostic stratospheric aerosol

136 module (Mills et al., 2016) and has been utilized extensively to study volcanic aerosols and their
137 impact on climate change and ozone losses (e.g., Mills et al., 2017; Stone et al., 2017; Zambri et
138 al., 2019). In this study, the simulations feature a horizontal resolution of 0.9° latitude $\times 1.25^\circ$
139 longitude using the finite volume dynamical core (Lin & Rood, 1996), and 110 vertical levels,
140 with a vertical resolution of $\sim 500\text{m}$ in the upper troposphere and lower stratosphere. WACCM6 is
141 run in a specified dynamics configuration (WACCM6-SD), where the temperatures and winds are
142 relaxed to Modern-Era Retrospective analysis for Research and Applications Version 2 (MERRA-
143 2) reanalyses (Gelaro et al., 2017) using a relaxation time of 50 hours. This configuration starts
144 from 2007 until the end of 2022, using initial conditions from a long historical simulation
145 (Gettelman et al., 2019). Starting in January 2022, we conduct two cases: the experiment case with
146 full forcing (SO_2 and H_2O injection) from the HTHH eruption (as defined in Zhu et al., 2022) and
147 the control case with no forcing (no SO_2 or H_2O injection) from HTHH eruption. The difference
148 between these two nudged simulations gives information about the chemistry contribution to the
149 stratospheric ozone depletion after the HTHH eruption. We use the emission described in Zhu et
150 al. (2022), where 150 Tg of H_2O and 0.42 Tg of SO_2 are injected on January 15, 2022, from ~ 20
151 to 35 km.

152

153

154 **3. Results and Discussions**

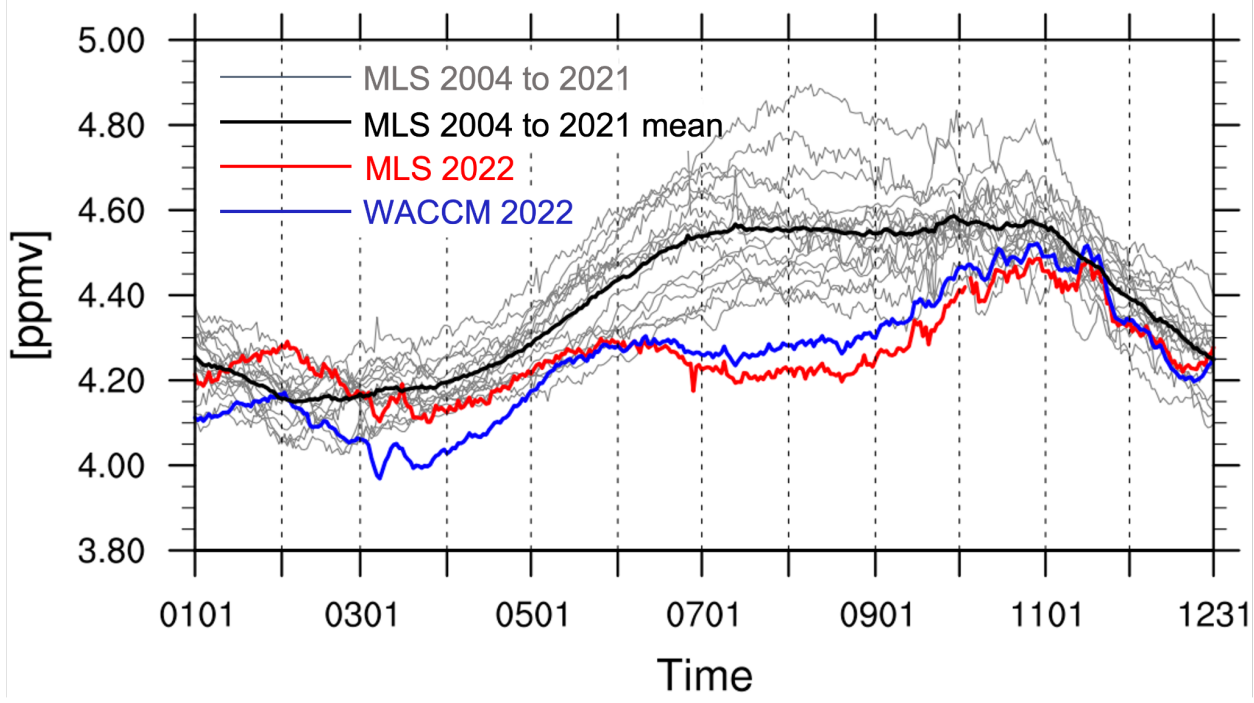
155 **3.1 Observed and simulated ozone anomaly from MLS and WACCM6-SD**

156

157 It is expected that the large HTHH H_2O and aerosol perturbations can impact stratospheric
158 dynamics and chemistry, and hence ozone abundances. Figure 1 shows MLS observed ozone from
159 2004 to 2022 and WACCM6-SD simulated ozone during 2022 in the stratosphere. MLS satellite
160 observations indicate anomalous negative ozone in 2022 both over SH midlatitudes and tropics
161 (10°S - 60°S) in winter as well as Antarctica (60°S - 82°S) in spring. The MLS ozone concentration
162 over 10°S - 60°S shows a record low relative to the climatology period (2004 to 2022) in the SH
163 austral winter (Fig. 1a, red line) at 30 hPa. Large midwinter interannual variability in this region
164 is linked to the Quasi-Biennial Oscillation (QBO), as discussed in Wang et al. (2023). MLS also
165 shows a relatively deep ozone hole in the SH austral spring (Fig. 1b) at 80 hPa. The negative ozone
166 anomaly over the polar region (60°S - 82°S) is large in October-December, but within the variability
167 of previous years. This is because the climatology period (2004 to 2022) also includes years with
168 either relatively strong polar vortex or volcanic impact. For example, the lowest line in Figure 1b
169 is in the year 2015, when a record October ozone hole occurred after the Calbuco volcanic eruption
170 (Solomon et al., 2015; Ivy et al., 2017). The accuracy of MLS O_3 is about 0.2 ppmv at 30 hPa and
171 0.1 ppmv near 80 hPa (Livesey et al., 2020). The difference between MLS climatology mean and
172 2022 is outside the MLS ozone systematic error during June-August in Fig. 1a and October in Fig.
173 1b, which reinforces the anomalous low ozone occurring in the SH mid-latitudes winter and
174 Antarctica spring 2022. WACCM6-SD captures both the record low ozone over 10°S - 60°S and
175 the large ozone anomaly over 60°S - 82°S , and is within the systematic error of MLS, except in
176 December 2022 in Fig. 1b.

177

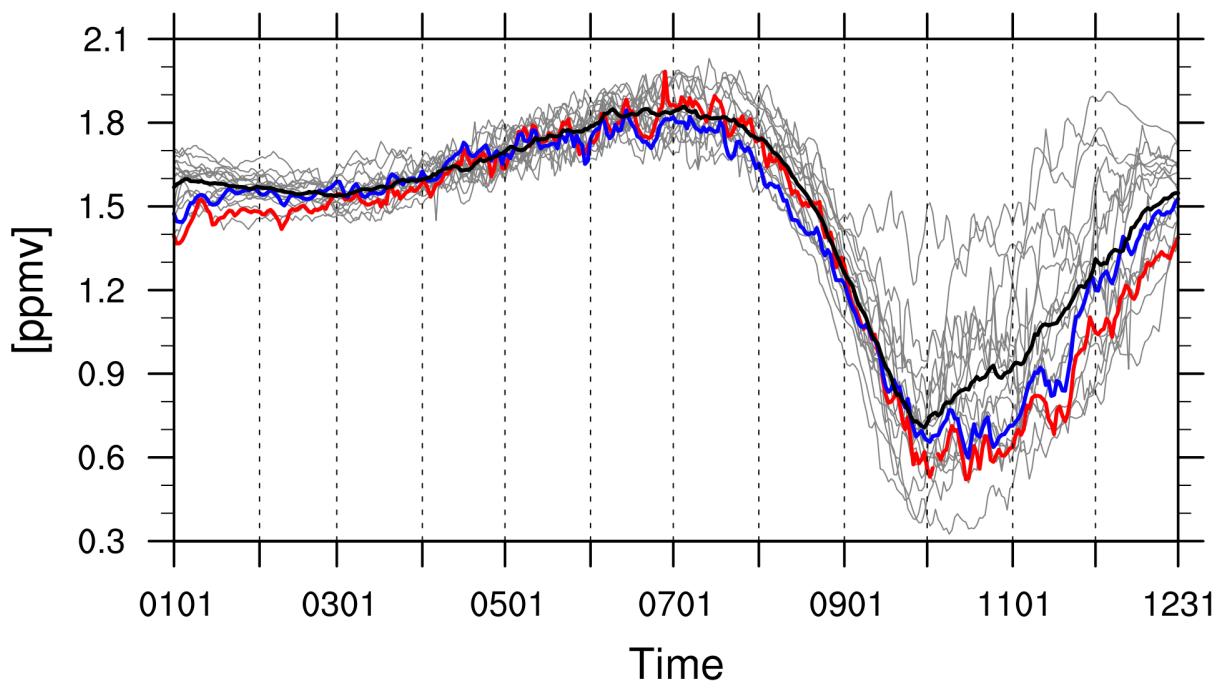
O₃@30hPa [60S-10S]



178

179

(a) O₃@80hPa [82S-60S]



180

181

182

183 **Figure 1.** Time series of ozone concentration (ppmv) for (a) midlatitudes and tropics (10°S-60°S)
184 at 30 hPa and (b) polar region (60°S-82°S) at 80 hPa from MLS and WACCM. MLS observations
185 are shown from 2004 to 2022. Gray lines show time serieses of MLS ozone during 2004-2021 and
186 the black line indicates the mean MLS ozone over the climatology. The red and blue lines are for
187 MLS and WACCM6-SD ozone in 2022, respectively.
188
189

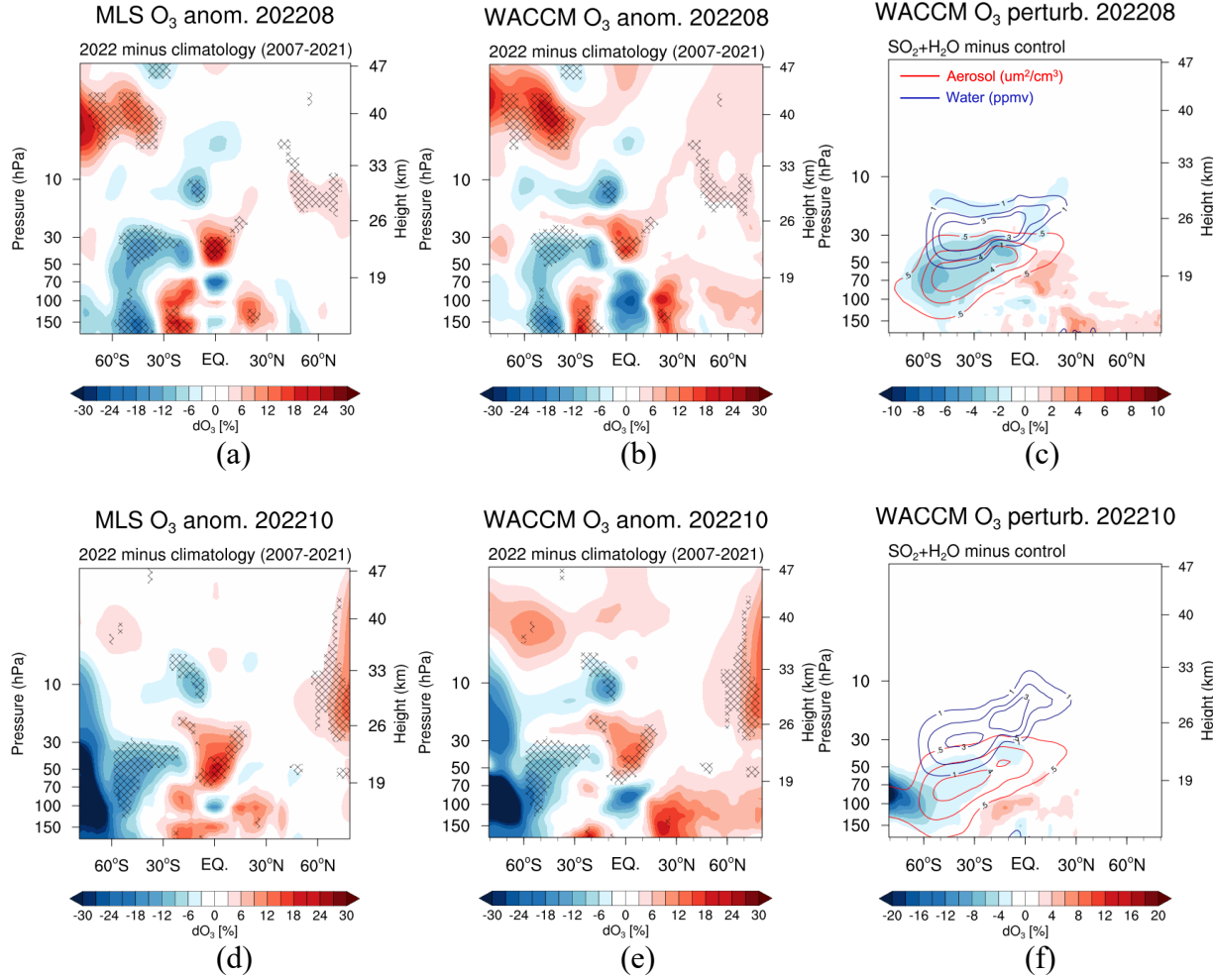
190 **3.2 Quantifying the chemical contribution to the ozone reduction**

191 Stratospheric ozone changes in 2022 compared with the climatology can be attributed to various
192 factors: internal variability in the climate system (e.g., QBO), and forced changes after the HTHH
193 eruption including both dynamics and chemistry impacts. Both observed and simulated 2022
194 anomalies showing in the following are calculated as deviations from the 2007-2021 background
195 instead of 2004-2021 to be consistent with model simulation period. We note that the difference
196 of the derived 2022 anomaly between using 2004 and 2007 is minimal. The derived ozone anomaly
197 from MLS and WACCM6-SD in August are shown in Figure 2a and 2b. The lower stratospheric
198 wintertime SH mid-latitude ozone reduction is well represented in WACCM6-SD, along with the
199 ozone increase in the tropics, which is related to the QBO. These ozone anomalies are the result
200 of the combination of internal variability and HTHH eruption forced changes. Figure 2c shows the
201 ozone changes due to chemistry only, calculated by taking the difference between the full forcing
202 experiment run ($\text{SO}_2 + \text{H}_2\text{O}$) and the no forcing control run in 2022. The blue and red contour lines
203 highlight the location of HTHH water and aerosol plumes, which reveals the separation of the H_2O
204 and aerosol plumes over time due to the sedimentation of the aerosols (Legras et al. 2022, Wang
205 et al., 2023). As the experiment and control simulations are nudged to the same dynamics, the
206 ozone changes in Figure 2c are purely due to the chemistry impact from the enhanced water and
207 aerosol SAD perturbation. The ozone depletion over the SH mid-latitudes ranges from 200 hPa up
208 to 30 hPa. In particular, the reduction at 30 to 50 hPa and 100 to 200 hPa are outside of previous
209 variability (hatched region), with the peak reaching about 20% ozone reduction. Chemistry only
210 contributes up to 6% of ozone depletion at mid-latitudes near 70 hPa (Fig. 2c). Consequently, less
211 than 30% of the ozone reduction at the hatched regions in Figure 2a and 2b is attributed to
212 chemistry, with the other changes a result of dynamical changes due to internal variability from
213 QBO and forced dynamical response to the HTHH eruption.
214

215 In the springtime (October-December) of the Antarctic polar region, a large negative ozone
216 anomaly is observed within the polar vortex (south of 60°S) in 2022 (Fig. 2d), even though it is
217 not a record-breaking low ozone hole (not hatched). WACCM6-SD reproduces this large ozone
218 reduction in general, but slightly underestimates the ozone loss between 30 to 50 hPa (Fig. 2e).
219 The simulation (Fig. 2f) shows that the aerosol plume from the HTHH eruption entered the
220 Antarctic near the bottom of the polar vortex (~100 hPa) in October. However, the water plume
221 was confined outside of the polar vortex due to the strong polar jet stream near 25 km (Schoeberl
222 et al. 2023; Manney et al. 2023; Wang et al., 2023). Note that although the simulated HTHH
223 aerosol penetrated across the bottom of the polar vortex, it is difficult to prove it with observations.
224 Enhanced polar extinction in OMPS-LP measurements can be due to polar stratospheric clouds in
225 the winter season (Manney et al., 2023; Wang et al., 2023). In addition, the amount of sulfate
226 entering the polar vortex in the simulation is relatively small (only double the background), and
227 satellite observations (e.g., CALIPSO lidar) sometimes cannot capture it due to background noise
228

229 level. The ozone depletion simulated in Figure 2f is because the volcanic aerosol entered the
 230 bottom of the polar vortex which provides additional SAD for heterogeneous chemistry in the
 231 polar region. Chemistry (Fig. 2f) leads to $\sim 20\%$ ozone reduction (this is equivalent to about 40%
 232 of the total ozone depletion) near the center of the Antarctic vortex.

233



234
 235
 236

237
 238
 239

240 **Figure 2.** Percentage change of 2022 ozone anomaly (%) relative to climatology (2007 to 2021)
 241 from MLS (a) and WACCM6-SD (b) in August. (d) and (e) are the same but for October. Hatched
 242 regions indicate where the 2022 anomalies are outside the range of all variability during 2007-
 243 2021. Percentage change of ozone (%) calculated from full-forcing ($\text{SO}_2+\text{H}_2\text{O}$) compared to no-
 244 forcing control runs in August (c) and October (f). The blue and red contour lines in (c) and (f)
 245 are water anomaly in ppmv and aerosol surface area density anomaly in um^2/cm^3 , respectively.
 246 Note that panel c and f have different color bar ranges from panel a, b, d, e.

247

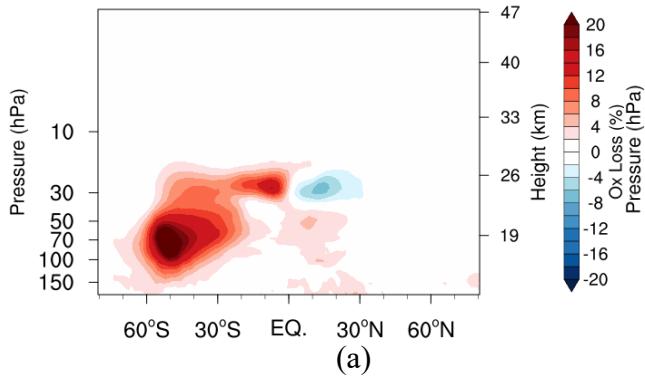
248 We characterize the major chemical processes that lead to the 6% and 20% of chemical ozone
 249 depletion in the mid-latitudes and polar regions discussed above. The chemical destruction of odd
 250 oxygen ($\text{Ox} = \text{O}_3 + \text{O} + \text{O}^{(1)\text{D}} + \text{other terms}$; Brasseur & Solomon, 2005) is directly linked to
 251 ozone abundance in the stratosphere. Different Ox catalytic destruction cycles involve nitrogen
 252 oxides (NOx-Ox), hydrogen radicals (HOx-Ox), halogen oxides (ClOx/BrOx-Ox) as well as the
 253 chemical loss by the Chapman self-destruction mechanism (Ox-Ox) (e.g., Crutzen & Ehhalt, 1977;

254 Solomon, 1999). Supplementary Text S1 defines the odd oxygen used in this study and the
255 reactions that are contained in each odd oxygen chemical family. Figure 3a and 3b characterize
256 the total Ox loss (sum of Ox-Ox, NOx-Ox, HOx-Ox and ClOx/BrOx-Ox cycles) during the SH
257 winter and spring. The changes in Ox are induced by the addition of water and aerosol injection
258 from HTHH eruption. In the wintertime, the major Ox loss occurs in the mid-latitudes from 150
259 to 20 hPa, consistent with the location of major ozone loss in Figure 2c. During springtime, the
260 total Ox loss extends into the polar region, associated with the aerosol plume shown in Figure 2f.
261

262 The vertical profile of changes in individual loss cycles are illustrated in Figure 3c and 3d for mid-
263 latitudes winter and Antarctic spring, respectively. Increasing aerosol surface areas decrease the
264 abundance of NOx and hence the NOx-catalyzed ozone destruction cycles (red lines) (discussed
265 in section 3.3). Both HOx-Ox and ClOx/BrOx-Ox cycles play important roles in the chemical
266 ozone destruction for mid-latitudes winter, but at different altitudes. The HOx-Ox cycle is more
267 significant at 20 to 30 km, while the ClOx/BrOx-Ox cycle plays a larger role below 20 km. The
268 enhanced HOx cycle is the combined results of direct water injection and the HOx repartitioning
269 induced from NOx reduction (Wennberg et al., 1994; Solomon et al., 1996). The reduced NOx
270 also gives rise to ClOx enhancement as ClOx is inversely correlated with NOx (Stimpfle et al.,
271 1994; Solomon et al., 1999). In the Antarctic spring, ClOx/BrOx-Ox cycle controls the behavior
272 of total Ox change below around 18 km. HOx-Ox loss cycle is still the major loss mechanism at
273 20 to 25 km. However, this loss is largely offset by hindered NOx-Ox loss, which is normally the
274 most important loss cycle at this altitude in the background atmosphere (Zhang et al., 2021). It is
275 eye-catching to see there is a negative Ox perturbation at around 16-18 km, corresponding to 70-
276 100 hPa in Figure 2b. This is because the ozone abundances in the experiment run drop to extreme
277 low values at 70-100 hPa in the core of the vortex, hence the formation of ClO (and therefore
278 chlorine nitrate ClONO₂) is impeded (Fig. S1). Rapid deactivation of Cl into hydrochloric acid
279 (HCl) then occurs even if the enhanced SAD are still present and temperatures are very cold
280 (Douglass et al., 1995; Solomon et al., 2015). This rapid deactivation suppresses the Ox loss due
281 to ClOx/BrOx-Ox cycle in the experiment run compared to the control run. Figure 3c and 3d
282 indicate that the reaction rates of all the Ox chemical loss cycles are modified even though only
283 SO₂ and H₂O emissions are injected into the atmosphere from the HTHH eruption. This is expected
284 since these cycles couple to each other and change repartitioning from each other.
285

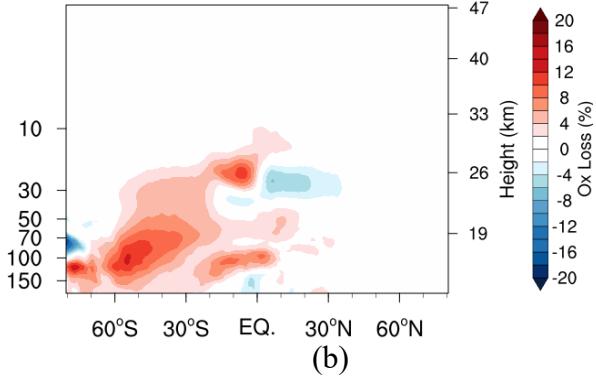
286
287

Total Odd Oxygen Loss 202208

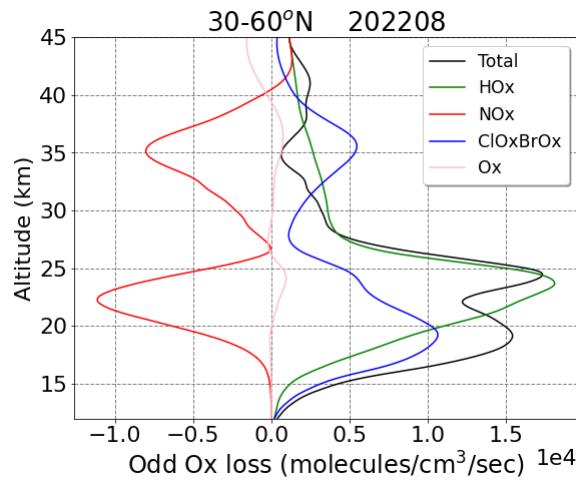


(a)

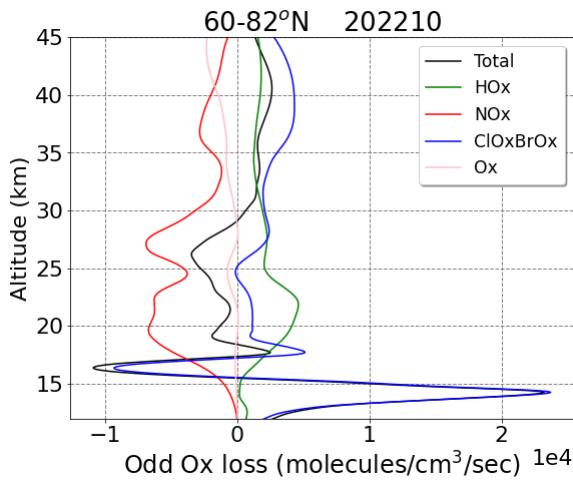
Total Odd Oxygen Loss 202210



(b)



(c)



(d)

288
289
290

291
292
293
294
295
296
297

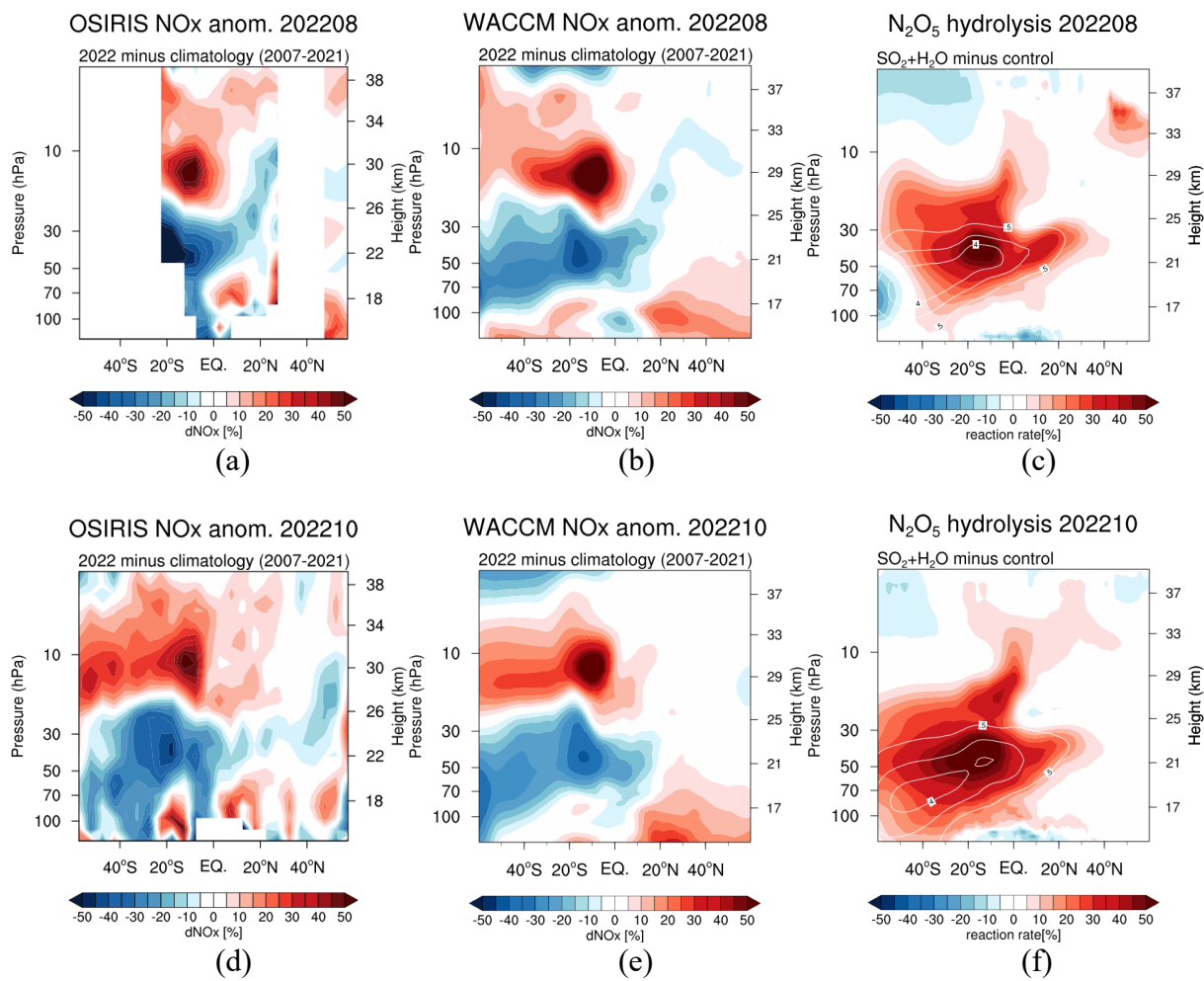
Figure 3. Calculated perturbations from full-forcing ($\text{SO}_2 + \text{H}_2\text{O}$) experiment run compared to no-forcing control run for total OddOx loss in August (a) and October (b). Vertical profile of total Odd oxygen (Ox) loss (in black) and the loss from individual cycles of HOx-Ox, NOx-Ox, ClOxBrOx-Ox and Ox-Ox at mid-latitudes in August (c) and Antarctic region in October (d).

298 3.3 Negative NOx anomaly after HTHH eruption

299
300
301
302
303
304
305
306
307
308
309
310

NOx reduction is expected following large volcanic eruptions, which perturbs ozone abundance in the stratosphere (e.g., Fahey et al., 1993; Mills et al., 1993; Berthet et al., 2017; Zambri et al., 2019). Figure 4 examines the NOx anomaly after the HTHH eruption from OSIRIS observations and WACCM6-SD model simulations. A dipole pattern is observed both in the OSIRIS and WACCM: a NOx reduction at around 25 km and below, and a positive anomaly above. This positive anomaly is mainly due to the QBO internal variability, as it is also seen in 2008 when the QBO phase is similar to 2022 while the negative anomaly is not found (Fig. S2) (Park et al., 2017). Figure 4a and 4d show the OSIRIS observed NOx anomalies in August and October 2022, with reductions of 30~40% over the mid-latitude lower stratosphere. This negative anomaly is approximately collocated with the HTHH aerosol plume in Figure 2c and 2f, which is consistent with the plume location shown in Wang et al. (2023) from the OMPS-LP data. The HTHH aerosol

311 reduce the NO_x abundance via the well-known heterogeneous chemical reactions dinitrogen
 312 pentoxide (N₂O₅) hydrolysis on aerosols (e.g., Hofmann and Solomon, 1989; Solomon, 1999;
 313 Berthet et al., 2017). Due to the N₂O₅ hydrolysis on the surface of aerosol, nitric acid (HNO₃)
 314 formation is promoted which acts as a major sink of NO_x in the atmosphere during night-time. We
 315 note that OSIRIS data show strong NO_x decreases throughout 2022 (not shown) that overlap the
 316 HTHH aerosol layer, but OSIRIS does not have high latitude measurements during midwinter.
 317 Model calculations (Fig. 4b and 4e) show NO_x decreases in the lower stratosphere that are similar
 318 in magnitude (~30-40%) and location to the OSIRIS results, demonstrating that the NO_x-aerosol
 319 reactions are captured well in the model. Figure 4c and 4f denote the modeled changes in N₂O₅
 320 hydrolysis rate overlying with aerosol SAD anomaly due to the HTHH eruption, derived from the
 321 difference between full-forcing (SO₂+H₂O) and no-forcing control runs. This heterogeneous
 322 chemical reaction rate is enhanced by more than 50% at the location where the maximum of NO_x
 323 reduction occurs in Figure 4b and 4e. The results shown here are consistent with the conclusion
 324 drawn from Santee et al. (2023) using MLS data, suggesting the hydrolysis of N₂O₅ is the primary
 325 mechanism for the reduction of NO_x. We note that even though this NO_x reduction is significant,
 326 we found that the NO_x impact on ozone is largely canceled by HO_x-Ox and ClO_x-Ox cycles as
 327 shown in Figure 3c and 3d.
 328



329
 330
 331

332
 333
 334

335 **Figure 4.** Calculated NO_x anomaly (%) relative to climatology (2007 to 2021) from OSIRIS and
336 WACCM6-SD in August and October (a), (b) and (d), (e). Calculated changes (%) in N₂O₅
337 hydrolysis rate on sulfate aerosols in the WACCM6-SD model from full-forcing (SO₂+H₂O)
338 compared to no-forcing control runs in August and October (c) and (f). The white contour line in
339 (c) and (f) is the aerosol surface area density anomaly in um²/cm³.
340

341 **4. Summary and discussion**

343 The January 2022 Hunga Tonga-Hunga Ha'apai eruption injected ~150 Tg of water and ~0.42 Tg
344 SO₂ into the SH stratosphere. MLS observed ozone reductions in the SH stratosphere mid-latitudes
345 and Antarctica during the 2022 austral wintertime and springtime. This work focuses on examining
346 and quantifying the chemical ozone depletion due to the SO₂ and H₂O injection. We use
347 WACCM6-SD nudged simulations to disentangle the role of chemistry from that of dynamics.
348 WACCM6-SD shows a good agreement with MLS ozone anomaly and also reproduces the NO_x
349 anomaly in 2022 compared to OSIRIS measurements.
350

351 We found chemistry contributes to 6% and 20% ozone depletion at mid-latitudes and Antarctica,
352 respectively. The majority of ozone changes are due to transport and dynamical processes from
353 internal variability in the climate system and forced response by the HTHH eruption. One caveat
354 is that the chemistry quantified here does not include the dynamics feedback on the chemistry. For
355 example, water can cool the stratosphere, which would further promote heterogeneous reactions.
356 However, because these two simulations conducted here are nudged to the same dynamics, the
357 temperature is not allowed to change to reflect the feedback on chemistry. To characterize the
358 chemical processes that contributed to the ozone loss, different loss cycles (NO_x-Ox, HO_x-Ox,
359 ClO_x/BrO_x-Ox and Ox-Ox) were examined and their relative significance to the ozone depletion
360 at SH mid-latitudes and Antarctica were evaluated. We found both HO_x-Ox and ClO_x/BrO_x-Ox
361 cycles play important roles in the total chemical ozone destruction for mid-latitudes winter. While
362 during the Antarctic spring, ClO_x/BrO_x-Ox cycle is dominant and controls the behavior of total
363 Ox change in the lower stratosphere. We also document that both OSIRIS and WACCM6-SD
364 show a NO_x reduction that collocates with HTHH aerosols plume, demonstrating the enhanced
365 N₂O₅ hydrolysis on sulfate aerosol. Consequently, the NO_x-Ox loss cycle is strongly suppressed
366 associated with the significant NO_x reduction. However, the NO_x impact on ozone is minimal
367 since it is largely canceled by HO_x-Ox and ClO_x/BrO_x-Ox cycles.
368
369

370 **Acknowledgments**

371 Jun Zhang and Xinyue Wang are supported by the NSF via NCAR's Advanced Study Program
372 Postdoctoral Fellowship. Douglas Kinnison is partially supported by NASA grant no.
373 80NSSC19K0952. NCAR's Community Earth System Model project is supported primarily by the
374 National Science Foundation. This material is based upon work supported by the National Center
375 for Atmospheric Research, which is a major facility sponsored by the NSF under Cooperative
376 Agreement No. 1852977. Computing and data storage resources, including the Cheyenne
377 supercomputer (doi:10.5065/D6RX99HX), were provided by the Computational and Information
378 Systems Laboratory (CISL) at NCAR. The authors thank the Swedish National Space Agency and
379 the Canadian Space Agency for the continued operation and support of Odin-OSIRIS. Kimberlee
380

381 Dube is supported by the Canadian Space Agency (grant no. 21SUASULSO). This project
382 received funding from NOAA's Earth Radiation Budget (ERB) Initiative (CPO #03-01-07-001).
383 Yunqian Zhu is supported in part by NOAA cooperative agreements NA17OAR4320101 and
384 NA22OAR4320151.

385

386

387 **Open Research**

388

389 CESM2/WACCM6 is an open-source community model, which was developed with support
390 primarily from the National Science Foundation. WACCM6 source code can be downloaded at
391 <https://www.cesm.ucar.edu/models/cesm2/download>. Figures in this study are plotted by using
392 NCAR Command Language (NCL) and Python. The related code can be found in NCL application
393 examples (<https://www.ncl.ucar.edu/Applications/>). Python is an open-source programming
394 language.

395

396

397 **References**

398

399 Anderson, J. G., Wilmouth, D. M., Smith, J. B., & Sayres, D. S. (2012). UV dosage levels in
400 summer: Increased risk of ozone loss from convectively injected water vapor. *Science*,
401 337(6096), 835-839. DOI: 10.1126/science.1222978. DOI: 10.1126/science.1222978

402

403 Berthet, G., Jégou, F., Catoire, V., Krysztofiak, G., Renard, J. B., Bourassa, A. E., ... & Guimbaud,
404 C. (2017). Impact of a moderate volcanic eruption on chemistry in the lower stratosphere:
405 balloon-borne observations and model calculations. *Atmospheric Chemistry and Physics*,
406 17(3), 2229-2253. <https://doi.org/10.5194/acp-17-2229-2017>

407

408 Brasseur, G. P., & Solomon, S. (2005). Aeronomy of the middle atmosphere: Chemistry and
409 physics of the stratosphere and mesosphere (Vol. 32). *Springer Science & Business Media*.

410

411 Carn, S. A., Krotkov, N. A., Fisher, B. L., & Li, C. (2022). Out of the blue: Volcanic SO₂ emissions
412 during the 2021–2022 eruptions of Hunga Tonga—Hunga Ha’apai (Tonga). *Frontiers in*
413 *Earth Science*, 10, 976962. <https://doi.org/10.3389/feart.2022.976962>

414

415 Carr, J. L., Horváth, Á., Wu, D. L., & Friberg, M. D. (2022). Stereo plume height and motion
416 retrievals for the record-setting Hunga Tonga-Hunga Ha'apai eruption of 15 January 2022.
417 *Geophysical Research Letters*, 49(9), e2022GL098131.
418 <https://doi.org/10.1029/2022GL098131>

419

420 Crutzen, P. J., & Ehhalt, D. H. (1977). Effects of nitrogen fertilizers and combustion on the
421 stratospheric ozone layer. *Ambio*, 112-117.

422

423 Douglass, A. R., Schoeberl, M. R., Stolarski, R. S., Waters, J. W., Russell III, J. M., Roche, A. E.,
424 & Massie, S. T. (1995). Interhemispheric differences in springtime production of HCl and
425 ClONO₂ in the polar vortices. *Journal of Geophysical Research: Atmospheres*, 100(D7),
426 13967-13978. <https://doi.org/10.1029/95JD00698>

- 427
428 Dubé, K., Randel, W., Bourassa, A., Zawada, D., McLinden, C., & Degenstein, D. (2020). Trends
429 and variability in stratospheric NO_x derived from merged SAGE II and OSIRIS satellite
430 observations. *Journal of Geophysical Research: Atmospheres*, 125(7), e2019JD031798.
431 <https://doi.org/10.1029/2019JD031798>
- 432
433 Dubé, K., Zawada, D., Bourassa, A., Degenstein, D., Randel, W., Flittner, D., Sheese, P., and
434 Walker, K.: An improved OSIRIS NO₂ profile retrieval in the upper troposphere–lower
435 stratosphere and intercomparison with ACE-FTS and SAGE III/ISS, *Atmos. Meas. Tech.*,
436 15, 6163–6180, <https://doi.org/10.5194/amt-15-6163-2022>, 2022.
- 437
438 Fahey, D. W., Kawa, S. R., Woodbridge, E. L., Tin, P., Wilson, J. C., Jonsson, H. H., ... & Chan,
439 K. R. (1993). In situ measurements constraining the role of sulphate aerosols in mid-
440 latitude ozone depletion. *Nature*, 363(6429), 509-514. <https://doi.org/10.1038/363509a0>
- 441
442 Gelaro, R., McCarty, W., Suárez, M. J., Todling, R., Molod, A., Takacs, L., ... & Zhao, B. (2017).
443 The modern-era retrospective analysis for research and applications, version 2 (MERRA-
444 2). *Journal of climate*, 30(14), 5419-5454. <https://doi.org/10.1175/JCLI-D-16-0758.1>
- 445
446 Gettelman, A., Mills, M. J., Kinnison, D. E., Garcia, R. R., Smith, A. K., Marsh, D. R., ... &
447 Randel, W. J. (2019). The whole atmosphere community climate model version 6
448 (WACCM6). *Journal of Geophysical Research: Atmospheres*, 124(23), 12380-12403.
449 <https://doi.org/10.1029/2019JD030943>
- 450
451 Hofmann, D. J., & Solomon, S. (1989). Ozone destruction through heterogeneous chemistry
452 following the eruption of El Chichon. *Journal of Geophysical Research: Atmospheres*,
453 94(D4), 5029-5041. <https://doi.org/10.1029/JD094iD04p05029>
- 454
455 Khaykin, S., Podglajen, A., Ploeger, F., Grooß, J. U., Tencé, F., Bekki, S., ... & Ravetta, F. (2022).
456 Global perturbation of stratospheric water and aerosol burden by Hunga eruption.
457 *Communications Earth & Environment*, 3(1), 316. <https://doi.org/10.1038/s43247-022-00652-x>
- 458
459 Kinnison, D. E., Grant, K. E., Connell, P. S., Rotman, D. A., & Wuebbles, D. J. (1994). The
460 chemical and radiative effects of the Mount Pinatubo eruption. *Journal of Geophysical
461 Research: Atmospheres*, 99(D12), 25705-25731. <https://doi.org/10.1029/94JD02318>
- 462
463 Krueger, A. J., Walter, L. S., Bhartia, P. K., Schnetzler, C. C., Krotkov, N. A., Sprod, I. T., &
464 Bluth, G. J. S. (1995). Volcanic sulfur dioxide measurements from the total ozone mapping
465 spectrometer instruments. *Journal of Geophysical Research: Atmospheres*, 100(D7),
466 14057-14076. <https://doi.org/10.1029/98GL00178>
- 467
468 Ivy, D. J., Solomon, S., Kinnison, D., Mills, M. J., Schmidt, A., & Neely III, R. R. (2017). The
469 influence of the Calbuco eruption on the 2015 Antarctic ozone hole in a fully coupled
470 chemistry-climate model. *Geophysical Research Letters*, 44(5), 2556-2561.
471 <https://doi.org/10.1002/2016GL071925>
- 472

- 473
474 Legras, B., Duchamp, C., Sellitto, P., Podglajen, A., Carboni, E., Siddans, R., ... & Ploeger, F.
475 (2022). The evolution and dynamics of the Hunga Tonga–Hunga Ha'apai sulfate aerosol
476 plume in the stratosphere. *Atmospheric Chemistry and Physics*, 22(22), 14957–14970.
477 <https://doi.org/10.5194/acp-22-14957-2022>
478
479 Lin, S. J., & Rood, R. B. (1996). Multidimensional flux-form semi-Lagrangian transport schemes.
480 *Monthly Weather Review*, 124(9), 2046–2070. [https://doi.org/10.1175/1520-0493\(1996\)124<2046:MFFSLT>2.0.CO;2](https://doi.org/10.1175/1520-0493(1996)124<2046:MFFSLT>2.0.CO;2)
481
482 Livesey, N J, W G Read, P A Wagner, L Froidevaux, M L Santee, and M J Schwartz. 2020.
483 “Version 5.0 x Level 2 and 3 Data Quality and Description Document (Tech. Rep. No. JPL
484 D-105336 Rev. A).” *Jet Propulsion Laboratory*.
485
486 Llewellyn, E. J., Lloyd, N. D., Degenstein, D. A., Gattinger, R. L., Petelina, S. V., Bourassa, A.
487 E., Wiensz, J. T., Ivanov, E. V., McDade, I. C., Solheim, B. H., McConnell, J. C., Haley,
488 C. S., von Savigny, C., Sioris, C. E., McLinden, C. A., Griffioen, E., Kaminski, J., Evans,
489 W. F., Puckrin, E., Strong, K., Wehrle, V., Hum, R. H., Kendall, D. J., Matsushita, J.,
490 Murtagh, D. P., Brohede, S., Stegman, J., Witt, G., Barnes, G., Payne, W. F., Piché, L.,
491 Smith, K., Warshaw, G., Deslauniers, D. L., Marchand, P., Richardson, E. H., King, R. A.,
492 Wevers, I., McCreath, W., Kyrölä, E., Oikarinen, L., Leppelmeier, G. W., Auvinen, H.,
493 Mégie, G., Hauchecorne, A., Lefèvre, F., de La Nöe, J., Ricaud, P., Frisk, U., Sjoberg, F.,
494 von Schéele, F., and Nordh, L.: The OSIRIS instrument on the Odin spacecraft, *Can. J.
495 Phys.*, 82, 411–422, <https://doi.org/10.1139/p04-005>, 2004.
496
497 Lu, J., Lou, S., Huang, X., Xue, L., Ding, K., Liu, T., ... & Ding, A. (2023). Stratospheric Aerosol
498 and Ozone Responses to the Hunga Tonga-Hunga Ha'apai Volcanic Eruption. *Geophysical
499 Research Letters*, 50(4), e2022GL102315. <https://doi.org/10.1029/2022GL102315>
500
501 Manney, G. L., Santee, M. L., Lambert, A., Millan, L., Minschwaner, K., Werner, F., ... & Wang,
502 T. (2023). Siege of the South: Hunga Tonga-Hunga Ha'apai Water Vapor Excluded from
503 2022 Antarctic Stratospheric Polar Vortex. *Authorea Preprints*.
504 10.22541/essoar.168057560.00140372/v1
505
506 McLinden, C. A., Olsen, S. C., Hannegan, B., Wild, O., Prather, M. J., & Sundet, J. (2000).
507 Stratospheric ozone in 3-D models: A simple chemistry and the cross-tropopause flux.
508 *Journal of Geophysical Research*, 105(D11), 14653–14665.
509 <https://doi.org/10.1029/2000JD900124>
510
511 Mills, M. J., Langford, A. O., O'Leary, T. J., Arpag, K., Miller, H. L., Proffitt, M. H., ... &
512 Solomon, S. (1993). On the relationship between stratospheric aerosols and nitrogen
513 dioxide. *Geophysical research letters*, 20(12), 1187–1190.
514 <https://doi.org/10.1029/93GL01124>
515
516 Mills, M. J., Schmidt, A., Easter, R., Solomon, S., Kinnison, D. E., Ghan, S. J., ... & Gettelman,
517 A. (2016). Global volcanic aerosol properties derived from emissions, 1990–2014, using

- 519 CESM1 (WACCM). *Journal of Geophysical Research: Atmospheres*, 121(5), 2332-2348.
520 <https://doi.org/10.1002/2015JD024290>
- 521
- 522 Mills, M. J., Richter, J. H., Tilmes, S., Kravitz, B., MacMartin, D. G., Glanville, A. A., ... &
523 Kinnison, D. E. (2017). Radiative and chemical response to interactive stratospheric sulfate
524 aerosols in fully coupled CESM1 (WACCM). *Journal of Geophysical Research: Atmospheres*,
525 122(23), 13-061. <https://doi.org/10.1002/2017JD027006>
- 526
- 527 Millan, L., Santee, M. L., Lambert, A., Livesey, N. J., Werner, F., Schwartz, M. J., ... &
528 Froidevaux, L. (2022). The Hunga Tonga-Hunga Ha'apai hydration of the stratosphere.
529 *Geophysical Research Letters*, 49(13), e2022GL099381.
530 <https://doi.org/10.1029/2022GL099381>
- 531
- 532 Murtagh, D., Frisk, U., Merino, F., Ridal, M., Jonsson, A., Stegman, J., Witt, G., Eriksson, P.,
533 Jiménez, C., Megie, G., Noë, J. d. l., Ricaud, P., Baron, P., Pardo, J. R., Hauchcorne, A.,
534 Llewellyn, E. J., Degenstein, D. A., Gattinger, R. L., Lloyd, N. D., Evans, W. F., McDade,
535 I. C., Haley, C. S., Sioris, C., Savigny, C. v., Solheim, B. H., McConnell, J. C., Strong, K.,
536 Richardson, E. H., Leppelmeier, G. W., Kyrölä, E., Auvinen, H., and Oikarinen, L.: An
537 overview of the Odin atmospheric mission, *Can. J. Phys.*, 80, 309–319,
538 <https://doi.org/10.1139/p01-157>, 2002.
- 539
- 540 Park, M., Randel, W. J., Kinnison, D. E., Bourassa, A. E., Degenstein, D. A., Roth, C. Z., ... &
541 Santee, M. L. (2017). Variability of stratospheric reactive nitrogen and ozone related to the
542 QBO. *Journal of Geophysical Research: Atmospheres*, 122(18), 10-103.
543 <https://doi.org/10.1002/2017JD027061>
- 544
- 545 Portmann, R. W., Solomon, S., Garcia, R. R., Thomason, L. W., Poole, L. R., & McCormick, M.
546 P. (1996). Role of aerosol variations in anthropogenic ozone depletion in the polar regions.
547 *Journal of Geophysical Research: Atmospheres*, 101(D17), 22991-23006.
548 <https://doi.org/10.1029/96JD02608>
- 549
- 550 Prather, M., & Jaffe, A. H. (1990). Global impact of the Antarctic ozone hole: Chemical
551 propagation. *Journal of Geophysical Research*, 95(D4), 3473–3492.
552 <https://doi.org/10.1029/JD095iD04p03473>
- 553
- 554 Proud, S. R., Prata, A. T., & Schmauß, S. (2022). The January 2022 eruption of Hunga Tonga-
555 Hunga Ha'apai volcano reached the mesosphere. *Science*, 378(6619), 554-557. DOI:
556 10.1126/science.abo4076
- 557
- 558 Randel, W. J., Johnston, B. R., Braun, J. J., Sokolovskiy, S., Vömel, H., Podglajen, A., & Legras,
559 B. (2023). Stratospheric Water Vapor from the Hunga Tonga–Hunga Ha’apai Volcanic
560 Eruption Deduced from COSMIC-2 Radio Occultation. *Remote Sensing*, 15(8), 2167.
561 <https://doi.org/10.3390/rs15082167>
- 562

- 563 Read, W. G., Froidevaux, L., & Waters, J. W. (1993). Microwave limb sounder measurement of
564 stratospheric SO₂ from the Mt. Pinatubo Volcano. *Geophysical Research Letters*, 20(12),
565 1299-1302. <https://doi.org/10.1029/93GL00831>
- 566
- 567 Santee, M. L., Lambert, A., Froidevaux, L., Manney, G. L., Schwartz, M. J., Millan, L., ... & Fuller,
568 R. A. (2023). Strong Evidence of Heterogeneous Processing on Stratospheric Sulfate
569 Aerosol in the Extrapolar Southern Hemisphere Following the 2022 Hunga Tonga-Hunga
570 Ha'apai Eruption. *Authorea Preprints*. DOI: 10.22541/essoar.168500358.84889871/v1
- 571
- 572 Schoeberl, M. R., Wang, Y., Ueyama, R., Taha, G., Jensen, E., & Yu, W. (2022). Analysis and
573 impact of the Hunga Tonga-Hunga Ha'apai stratospheric water vapor plume. *Geophysical
574 Research Letters*, 49(20), e2022GL100248. <https://doi.org/10.1029/2022GL100248>
- 575
- 576 Stimpfle, R. M., Koplow, J. P., Cohen, R. C., Kohn, D. W., Wennberg, P. O., Judah, D. M., ... &
577 Chan, K. R. (1994). The response of ClO radical concentrations to variations in NO₂
578 radical concentrations in the lower stratosphere. *Geophysical research letters*, 21(23),
579 2543-2546. <https://doi.org/10.1029/94GL02373>
- 580
- 581 Stone, K. A., Solomon, S., Kinnison, D. E., Pitts, M. C., Poole, L. R., Mills, M. J., ... & Hagiya,
582 S. (2017). Observing the impact of Calbuco volcanic aerosols on South Polar ozone
583 depletion in 2015. *Journal of Geophysical Research: Atmospheres*, 122(21), 11-862.
584 <https://doi.org/10.1002/2017JD026987>
- 585
- 586 Solomon, S., Portmann, R. W., Garcia, R. R., Thomason, L. W., Poole, L. R., & McCormick, M.
587 P. (1996). The role of aerosol variations in anthropogenic ozone depletion at northern
588 midlatitudes. *Journal of Geophysical Research: Atmospheres*, 101(D3), 6713-6727.
589 <https://doi.org/10.1029/95JD03353>
- 590
- 591 Solomon, S., Borrmann, S., Garcia, R. R., Portmann, R., Thomason, L., Poole, L. R., ... &
592 McCormick, M. P. (1997). Heterogeneous chlorine chemistry in the tropopause region.
593 *Journal of Geophysical Research: Atmospheres*, 102(D17), 21411-21429.
594 <https://doi.org/10.1029/97JD01525>
- 595
- 596 Solomon, S., Portmann, R. W., Garcia, R. R., Randel, W., Wu, F., Nagatani, R., ... & McCormick,
597 M. P. (1998). Ozone depletion at mid-latitudes: Coupling of volcanic aerosols and
598 temperature variability to anthropogenic chlorine. *Geophysical Research Letters*, 25(11),
599 1871-1874. <https://doi.org/10.1029/98GL01293>
- 600
- 601 Solomon, S. (1999). Stratospheric ozone depletion: A review of concepts and history. *Reviews of
602 geophysics*, 37(3), 275-316. <https://doi.org/10.1029/1999RG900008>
- 603
- 604 Solomon, S., Portmann, R. W., Sasaki, T., Hofmann, D. J., & Thompson, D. W. (2005). Four
605 decades of ozonesonde measurements over Antarctica. *Journal of Geophysical Research:
606 Atmospheres*, 110(D21). <https://doi.org/10.1029/2005JD005917>
- 607

- 608 Solomon, S., Kinnison, D., Bandoro, J., & Garcia, R. (2015). Simulation of polar ozone depletion:
609 An update. *Journal of Geophysical Research: Atmospheres*, 120(15), 7958-7974.
610 <https://doi.org/10.1002/2015JD023365>
- 611
- 612 Solomon, S., Ivy, D. J., Kinnison, D., Mills, M. J., Neely III, R. R., & Schmidt, A. (2016).
613 Emergence of healing in the Antarctic ozone layer. *Science*, 353(6296), 269-274. DOI:
614 10.1126/science.aae0061
- 615
- 616 Stone, K. A., Solomon, S., Kinnison, D. E., Pitts, M. C., Poole, L. R., Mills, M. J., ... & Hagiya,
617 S. (2017). Observing the impact of Calbuco volcanic aerosols on South Polar ozone
618 depletion in 2015. *Journal of Geophysical Research: Atmospheres*, 122(21), 11-862.
619 <https://doi.org/10.1002/2017JD026987>
- 620
- 621 Taha, G., Loughman, R., Colarco, P. R., Zhu, T., Thomason, L. W., & Jaross, G. (2022). Tracking
622 the 2022 Hunga Tonga-Hunga Ha'apai aerosol cloud in the upper and middle stratosphere
623 using space-based observations. *Geophysical Research Letters*, 49(19), e2022GL100091.
624 <https://doi.org/10.1029/2022GL100091>
- 625
- 626 Tie, X., & Brasseur, G. (1995). The response of stratospheric ozone to volcanic eruptions:
627 Sensitivity to atmospheric chlorine loading. *Geophysical Research Letters*, 22(22), 3035-
628 3038. <https://doi.org/10.1029/95GL03057>
- 629
- 630 Vömel, H., Evan, S., & Tully, M. (2022). Water vapor injection into the stratosphere by Hunga
631 Tonga-Hunga Ha'apai. *Science*, 377(6613), 1444-1447. DOI: 10.1126/science.abq2299
- 632
- 633 Wang, X., Randel, W., Zhu, Y., Tilmes, S., Starr, J., Yu, W., ... & Li, J. (2022). Stratospheric
634 climate anomalies and ozone loss caused by the Hunga Tonga volcanic eruption. *Authorea
635 Preprints*. DOI: 10.1002/essoar.10512922.1
- 636
- 637 Wennberg, P. O., Cohen, R. C., Stimpfle, R. M., Koplow, J. P., Anderson, J. G., Salawitch, R.
638 J., ... & Wofsy, S. C. (1994). Removal of stratospheric O₃ by radicals: In situ measurements
639 of OH, HO₂, NO, NO₂, ClO, and BrO. *Science*, 266(5184), 398-404. DOI:
640 10.1126/science.266.5184.398
- 641
- 642 Xu, J., Li, D., Bai, Z., Tao, M., & Bian, J. (2022). Large amounts of water vapor were injected into
643 the stratosphere by the hunga tonga-hunga ha'apai volcano eruption. *Atmosphere*, 13(6),
644 912. <https://doi.org/10.3390/atmos13060912>
- 645
- 646 Zambri, B., LeGrande, A. N., Robock, A., & Slawinska, J. (2017). Northern Hemisphere winter
647 warming and summer monsoon reduction after volcanic eruptions over the last millennium.
648 *Journal of Geophysical Research: Atmospheres*, 122(15), 7971-7989.
649 <https://doi.org/10.1002/2017JD026728>
- 650
- 651 Zambri, B., Solomon, S., Kinnison, D. E., Mills, M. J., Schmidt, A., Neely III, R. R., ... & Roth,
652 C. Z. (2019). Modeled and observed volcanic aerosol control on stratospheric NO_y and

- 653 Cly. *Journal of Geophysical Research: Atmospheres*, 124(17-18), 10283-10303.
654 <https://doi.org/10.1029/2019JD031111>
- 655
- 656 Zhang, J., Wuebbles, D., Kinnison, D., & Baughcum, S. L. (2021). Stratospheric ozone and climate
657 forcing sensitivity to cruise altitudes for fleets of potential supersonic transport aircraft.
658 *Journal of Geophysical Research: Atmospheres*, 126(16), e2021JD034971.
659 <https://doi.org/10.1029/2021JD034971>
- 660
- 661 Zhu, Y., Toon, O. B., Kinnison, D., Harvey, V. L., Mills, M. J., Bardeen, C. G., ... & Jégou, F.
662 (2018). Stratospheric aerosols, polar stratospheric clouds, and polar ozone depletion after
663 the Mount Calbuco eruption in 2015. *Journal of Geophysical Research: Atmospheres*,
664 123(21), 12-308. <https://doi.org/10.1029/2018JD028974>
- 665
- 666 Zhu, Y., Bardeen, C. G., Tilmes, S., Mills, M. J., Wang, X., Harvey, V. L., ... & Toon, O. B.
667 (2022). Perturbations in stratospheric aerosol evolution due to the water-rich plume of the
668 2022 Hunga-Tonga eruption. *Communications Earth & Environment*, 3(1), 248.
669 <https://doi.org/10.1038/s43247-022-00580-w>
- 670
- 671